Strong-field approximation and its modifications as evolution equations

I. A. Ivanov,[1,2,*] Chang Hee Nam,[1,3] and Kyung Taec Kim[1,3,†]
[1]*Center for Relativistic Laser Science, Institute for Basic Science, Gwangju 61005, Korea*
[2]*Max Planck Institute for the Physics of Complex Systems, Noethnitzer Strasse 38, 01187 Dresden, Germany*
[3]*Department of Physics and Photon Science, GIST, Gwangju 61005, Korea*

(Received 26 November 2018; published 14 January 2019)

We describe an approach based on the view of the well-known strong-field approximation (SFA) as an evolution equation. From this point of view the SFA is a nonhomogeneous evolution equation with the inhomogeneous term which determines the departure of the approximate evolution driven by the SFA from the evolution driven by the exact *ab initio* time-dependent Schrödinger equation (TDSE). A modification of this nonhomogeneous evolution equation making the inhomogeneous term smaller produces results for the photoelectron spectra which agree quantitatively well with the TDSE results for a system with the Coulomb interaction (we use hydrogen as an example).

DOI: 10.1103/PhysRevA.99.013417

I. INTRODUCTION

The pioneering paper by Keldysh [1] laid a foundation for the nonperturbative description of the processes occurring when atoms and molecules interact with intense laser fields. The approach used by Keldysh relied on the so-called Volkov states [2], exact solutions of the time-dependent Schrödinger equation (TDSE) for an electron in the field of a plane monochromatic electromagnetic wave. This idea has been subsequently used to develop well-known theoretical approaches: strong-field approximation (SFA) [3,4] and Perelomov-Popov-Terentiev [5] methods. These methods provide a basis for the description of various ionization phenomena for the laser pulses of arbitrary polarization and atomic or molecular systems. An important advantage of these approaches is that they require only relatively little computational effort which makes them extremely useful, especially for the complicated target systems and the multiquantum processes, when the direct solution of the *ab initio* TDSE becomes a demanding computational task.

For the systems governed by the short-range interactions (e.g., the negative ions) and relatively weak driving electromagnetic fields, when one can neglect the depletion of the initial atomic state, this description is also quantitatively accurate, as long as we are interested in the so-called direct electrons which do not experience rescattering by the parent ion. Rescattering effects are responsible for the appearance of the high-energy above-threshold-ionization (HATI) electrons in the spectra and for the high-order harmonic generation (HHG) [6]. These effects can be taken into account either perturbatively [7,8] by considering atomic potential as a perturbation, or using the so-called quantitative rescattering theory (QRS) [6]. Alternatively, one can use the adiabatic theory of ionization [9], which takes into account both the depletion and rescattering effects and provides, therefore, a quantitatively accurate tool for studying ionization of the systems driven by the intense low-frequency electromagnetic fields with the only restriction that the field-free dynamics of the system in question should be governed by the short-range interactions.

For the practically important case of the ionization of neutral atoms or molecules, when the Coulomb potential of the ionic core affects the motion of the ionized electron to a considerable degree, application of the SFA or PPT methods can result in a considerable quantitative difference (which can reach, e.g., a few orders of magnitude for the total ionization probability) with the *ab initio* TDSE results. A number of approaches have been described in the literature which allow one to make these methods quantitatively accurate for the systems with the Coulomb potential, such as the Coulomb-Volkov approximation (CVA) [10–15], Coulomb-corrected ionization amplitude [16] obtained using the imaginary time method (ITM), or the analytic R-matrix (ARM) method [17].

In the present work we describe an approach based on the view of the SFA as an evolution equation. This view can be useful by itself since it, as we shall see, encapsulates in a concise form the main deficiencies of the SFA method. It also allows a modification which, as we show, agrees well with the *ab initio* TDSE for a system with the Coulomb interaction (we use hydrogen as an example).

II. THEORY

The approach we present below can be most concisely formulated using the notion of the unitary time-evolution operator $\hat{U}(t,\tau)$ which takes states of the system at time τ to the states at time t. For the reader's convenience we begin with recapitulating a few well-known facts.

For the system with the Hamiltonian operator $\hat{H}(t) = \hat{H}_A(t) + \hat{B}(t)$ the evolution operator satisfies the integral Dyson equations which can be written in two equivalent forms as

$$\hat{U}(t,0) = \hat{U}_A(t,0) - i\int_0^t \hat{U}_A(t,\tau)\hat{B}(\tau)\hat{U}(\tau,0)\,d\tau \qquad (1)$$

*igorivanov@ibs.re.kr
†kyungtaec@gist.ac.kr

and

$$\hat{U}(t,0) = \hat{U}_A(t,0) - i\int_0^t \hat{U}(t,\tau)\hat{B}(\tau)\hat{U}_A(\tau,0)\,d\tau, \quad (2)$$

where $\hat{U}_A(t,\tau)$ is the time-evolution operator describing evolution driven by the Hamiltonian operator $\hat{H}_A$.

Consider a Hamiltonian which describes an atomic or molecular system interacting with the electromagnetic field: $\hat{H}(t) = \hat{T} + \hat{V} + \hat{H}_{\rm int}(t)$, where $\hat{T}$ is the kinetic-energy operator, $\hat{V}$ the potential-energy operator, and $\hat{H}_{\rm int}(t)$ describes the interaction of the system and the electromagnetic field. Two useful partitions of this Hamiltonian $\hat{H}(t)$ are

$$\hat{H}(t) = \hat{H}_{\rm atom} + \hat{H}_{\rm int}(t) \quad (3)$$

and

$$\hat{H}(t) = \hat{H}_F(t) + \hat{V}, \quad (4)$$

where $\hat{H}_{\rm atom} = \hat{T} + \hat{V}$ is the field-free Hamiltonian of the system; $\hat{H}_F(t) = \hat{T} + \hat{H}_{\rm int}(t)$ is the so-called Volkov Hamiltonian. Using these two partitions in the Dyson equations (1), (2), one obtains two equations:

$$\hat{U}(t,0) = \hat{U}_0(t,0) - i\int_0^t \hat{U}(t,\tau)\hat{H}_{\rm int}(\tau)\hat{U}_0(\tau,0)\,d\tau \quad (5)$$

and

$$\hat{U}(t,0) = \hat{U}_F(t,0) - i\int_0^t \hat{U}_F(t,\tau)\hat{V}\hat{U}(\tau,0)\,d\tau, \quad (6)$$

where, assuming that the field-free Hamiltonian is time independent, $\hat{U}_0(t,\tau) = \exp\{-i\hat{H}_{\rm atom}(t-\tau)\}$, and the Volkov time-evolution operator is given by [18,19]

$$\hat{U}_F(t,\tau) = e^{i\boldsymbol{A}(t)\cdot\boldsymbol{r}}\exp\left\{-\frac{i}{2}\int_\tau^t (\hat{\boldsymbol{p}} + \boldsymbol{A}(x))^2\,dx\right\}e^{-i\boldsymbol{A}(\tau)\cdot\boldsymbol{r}}, \quad (7)$$

where we used the length form $\hat{H}_{\rm int}(t) = \boldsymbol{E}(t)\cdot\boldsymbol{r}$ [$\boldsymbol{E}(t)$ is the electric field] for the interaction Hamiltonian. We assume that the nonrelativistic dipole approximation is valid, i.e., electric field does not depend on the spatial variables and all magnetic interactions can be neglected. To keep the formulas simple we write all the equations for a system with one electron.

A. SFA as an inhomogeneous evolution equation

Equations (5) and (6) are exact but not very useful, since they are integral equations which are difficult to solve. If we substitute $\hat{U}_F(t,\tau)$ for $\hat{U}(t,\tau)$ under the integral in the Dyson equation (1) and $\hat{U}_0(\tau,0)$ for $\hat{U}(\tau,0)$ in the second equation (2), we obtain two widely used and important approximations:

$$\hat{U}_{SFA}(t,0) = \hat{U}_0(t,0) - i\int_0^t \hat{U}_F(t,\tau)\hat{H}_{\rm int}(\tau)\hat{U}_0(\tau,0)\,d\tau \quad (8)$$

and

$$\hat{U}_{PPT}(t,0) = \hat{U}_F(t,0) - i\int_0^t \hat{U}_F(t,\tau)\hat{V}\hat{U}_0(\tau,0)\,d\tau. \quad (9)$$

If one uses the approximate expression for the evolution operator in Eq. (8) to find the wave function at the time $t = T_1$ at the end of the laser pulse for a system which was initially in the field free state ϕ_0, one obtains an approximate wave function: $\Psi_{SFA}(T_1) = \hat{U}_{SFA}(T_1,0)\phi_0$. Projecting this wave function on a plane-wave state $|\boldsymbol{k}\rangle$ and dropping the term $\langle\boldsymbol{k}|\hat{U}_0(T_1,0)|\phi_0\rangle$, one obtains the well-known expression for the ionization amplitude used by Keldysh [1]. Had we used a velocity gauge for the interaction operator we would have obtained the expression for the ionization amplitude used in the well-known strong-field approximation (SFA) theory [3,4]. The difference between the two is only in the choice of the gauge [18]. This distinction is not very important for us in the following; we employed, therefore, the notation $\hat{U}_{SFA}(t,0)$ for the evolution operator in Eq. (8) even though we will use the length gauge for the interaction operator in the calculations below. Similarly, using the approximate evolution operator in Eq. (9) to evaluate the wave function at the time $t = T_1$ at the end of the laser pulse for a system which was initially in the field free state ϕ_0, one obtains an approximate wave function $\Psi_{PPT}(T_1) = \hat{U}_{PPT}(T_1,0)\phi_0$. Projecting this wave function on a plane-wave state $|\boldsymbol{k}\rangle$ and dropping the term $\langle\boldsymbol{k}|\hat{U}_F(T_1,0)|\phi_0\rangle$ which does not contribute to the probability current, one obtains the expression for the ionization amplitude used in the well-known Perelomov-Popov-Terentiev (PPT) theory [5].

The goal of the present work is to look at these approximations from the time-dependent point of view by considering them as evolution equations. Introducing the time-dependent wave function defined by the action of the SFA evolution operator (8) on the initial state ϕ_0:

$$\Psi_{SFA}(t) = \hat{U}_{SFA}(t,0)\phi_0, \quad (10)$$

using the expression (8) for the SFA evolution operator and the evolution equation $i\frac{\partial\hat{U}_F(t,\tau)}{\partial t} = \hat{H}_F(t)\hat{U}_F(t,\tau)$ for the Volkov propagator, we obtain from (8) and (10) the following evolution equation for $\Psi_{SFA}(t)$:

$$i\frac{\partial\Psi_{SFA}(t)}{\partial t} - \hat{H}_F(t)\Psi_{SFA}(t) = \hat{V}\phi_0 e^{-i\varepsilon_0 t}, \quad (11)$$

where ϕ_0 and ε_0 are initial-state wave function and energy, respectively. Equation (11) can also be written as

$$i\frac{\partial\Psi_{SFA}(t)}{\partial t} - \hat{H}(t)\Psi_{SFA}(t) = \hat{V}(\phi_0 e^{-i\varepsilon_0 t} - \Psi_{SFA}(t)). \quad (12)$$

Using Eq. (12) we can look at the SFA approximation from the time-dependent perspective, considering it as an evolution equation. One can see from Eq. (12) that from this perspective SFA is a nonhomogeneous equation. Presence of the nonhomogeneous term makes the evolution driven by Eq. (12) nonunitary, i.e., the norm $||\Psi_{SFA}(t)||$ is not preserved in time. For the solution of the nonhomogeneous evolution equation (12) to provide a good approximation to the solution of the true homogeneous TDSE, we must evidently require

$$||\hat{V}(\phi_0 e^{-i\varepsilon_0 t} - \Psi_{SFA}(t))|| \ll 1 \quad (13)$$

in the course of the evolution. This gives a formal criteria of the quantitative validity of the SFA approximation. To fulfill this criteria one can demand, for instance, the electric field to be not too strong and the atomic potential to be short ranged, so that the $|\phi_0 e^{-i\varepsilon_0 t} - \Psi_{SFA}(t)|$ is small in the region where potential V is non-negligible. These are, of course, the

well-known conditions one must impose on the field strength and atomic potential for the validity of the SFA approximation [18,20]. Equation (13) just encapsulates these conditions in a concise form.

We could repeat the same steps for the PPT time-dependent wave function which we can define by the relation $\Psi_{PPT}(t) = \hat{U}_{PPT}(t,0)\phi_0$, with the evolution operator given by Eq. (9). It turns out that we obtain in this way the same nonhomogeneous evolution equation (12) for the time-dependent wave function $\Psi_{PPT}(t)$. From the time-dependent point of view these approximations are identical. We shall, therefore, discuss only the time-dependent $\Psi_{SFA}(t)$ in the following.

As Eq. (13) shows, the time-dependent view of the SFA has some pedagogical value, allowing us to capture in a concise form the known results. The utility of the time-dependent perspective, however, can be extended further. We can, for instance, consider two evolution processes, one driven by the true TDSE and another driven by the nonhomogeneous TDSE (12), and try to see when the true TDSE and the nonhomogeneous TDSE wave functions begin to deviate. Our ultimate goal in following this program will be to try to modify the nonhomogeneous evolution equation (12) so that SFA becomes an accurate approximation even for a long-range potential and strong fields.

B. Solution of the homogeneous and inhomogeneous evolution equations

As an example, we consider below ionization of a hydrogen atom driven by a linearly polarized (with the polarization vector along z axis, which we assume to be the axis of quantization) laser pulse, which we define in terms of the vector potential $\boldsymbol{A}(t)$ as $\boldsymbol{E}(t) = -\frac{\partial \boldsymbol{A}(t)}{\partial t}$ with

$$\boldsymbol{A}(t) = -\hat{\boldsymbol{z}}\frac{E_0}{\omega}\sin^2\left\{\frac{\pi t}{T_1}\right\}\sin\omega t, \tag{14}$$

with peak field strength E_0, carrier frequency ω, and total duration $T_1 = NT$, where $T = 2\pi/\omega$ is an optical period (o.c.) corresponding to the carrier frequency ω, with $N \in \mathbb{N}$. In the calculation we present below we will use the carrier frequency $\omega = 0.057$ a.u. and we will vary the peak's field strength E_0 and the total pulse duration T_1. To solve the true homogenous TDSE:

$$i\frac{\partial \Psi_{TDSE}(t)}{\partial t} - (\hat{H}_{\rm atom} + \hat{H}_{\rm int}(t))\Psi_{TDSE}(t) = 0, \tag{15}$$

where we use the length form $\hat{H}_{\rm int}(t) = \boldsymbol{E}(t)\cdot\boldsymbol{r}$, we follow the procedure described in detail in our previous works [21,22]. We give therefore only the necessary details of the calculation. The wave function is represented in the form

$$\Psi(\boldsymbol{r},t) = \sum_{l=0}^{l_{\rm max}}\frac{f_l(r,t)}{r}Y_{l0}(\hat{\boldsymbol{r}}), \tag{16}$$

where the radial variable is discretized on the grid with the step size $\delta r = 0.1$ a.u. in a box of the size $R_{\rm max}$. We used $R_{\rm max} = 800$ a.u. in the calculations below. As for the parameter $l_{\rm max}$ in Eq. (16), its value affects the convergence of the expansion (16) and therefore, ultimately, the accuracy of the calculation. After the necessary convergence checks we chose the value $l_{\rm max} = 60$ which was sufficient to achieve convergence for the highest peak field strength $E_0 = 0.1$ a.u. we consider below. Upon substituting expansion (16) in the homogeneous TDSE (15) one obtains a system of the coupled equations for the radial functions $f_l(r,t)$ which is solved using the matrix iteration method (MIM) [23,24]. To solve the inhomogeneous evolution equation (12) we follow a similar procedure. We employ again expansion (16) and a straightforward modification of the MIM method suitable for the case of the inhomogeneous evolution equation. The ionization amplitudes in both calculations are found by computing the Coulomb transform of a wave function $\Psi(T_1)$ [where $\Psi(T_1)$ can be either $\Psi_{TDSE}(T_1)$ or $\Psi_{SFA}(T_1)$] at the end of the pulse, i.e., by projecting it on the set of the scattering states of hydrogen:

$$a_{\boldsymbol{q}}^{CP} = \langle\phi_{\boldsymbol{q}}^{-}|\Psi(T_1)\rangle, \tag{17}$$

where CP stands for the Coulomb projection, $\phi_{\boldsymbol{q}}$ is an ingoing scattering state, and we use $\delta(\boldsymbol{q}-\boldsymbol{q}')$ normalization for the scattering states. With this normalization the differential ionization probability is $P(\boldsymbol{q}) = |a_{\boldsymbol{q}}^{CP}|^2$. Note that here we differ somewhat from the usual prescriptions of the SFA or PPT methods, where projection on the plane-wave basis set is used. Our aim, however, is to compare the results given by the TDSE and the SFA procedures (and its modification which we present below). To make such a comparison fully meaningful we have to project the wave functions on the same set of the final states which we chose, following the usual prescription, to be the ingoing scattering states of hydrogen. To avoid any possible confusion we shall adopt below an abbreviation SFA CP (SFA with the Coulomb projection) for the results obtained using projection of the solution of the SFA evolution equation (12) taken at the end of the pulse on the set of the hydrogen scattering states.

Results which the TDSE and SFA CP calculations give for the total ionization probabilities for different peak field strengths and pulse durations are presented in Table I. The results illustrate the well-known fact that for the systems with long-range (Coulomb potential) SFA can easily be off the mark by a few orders of magnitude. Note that for the same field strength the total ionization probabilities for the very short pulse of the 2 o.c. duration can be higher than for the longer pulse of the 4 o.s. duration. This is a well-known effect [25] due to the large spectral width of a very short pulse.

The dynamic approach which we use here allows us to see in more detail when the SFA and the TDSE wave functions evolving from the same initial ground state of the hydrogen atom begin to deviate significantly. The norm of the difference of the state vectors Ψ_{TDSE} and Ψ_{SFA}, evolving from the same initial ground state of hydrogen according to the evolution equations (15) and (12), correspondingly, is shown as a function of time in Fig. 1. The driving laser pulse has the peak strength $E_0 = 0.0534$ a.u. and the total duration $T_1 = 2$ o.c.

As one can see from Fig. 1, the squared norm $||\Psi_{TDSE} - \Psi_{SFA}||^2$ experiences fast growth at times near the local maxima of the field. Expectedly, these are the times at which the norm of the difference $\Psi_{SFA} - \phi_0 e^{-i\varepsilon_0 t}$, which forms the inhomogeneous term on the right-hand side of Eq. (12), has local maxima. To minimize the deviation of the approximate

TABLE I. Total ionization probabilities given by the TDSE, SFA, and SFAM calculations.

E_0 (a.u.)	Pulse duration (o.c.)	TDSE	SFA CP	SFAM CP	SFAM PW
0.03	2	2.07×10^{-5}	2.00×10^{-7}	1.971×10^{-5}	1.974×10^{-5}
0.0534	2	5.08×10^{-3}	1.73×10^{-4}	4.73×10^{-3}	4.74×10^{-3}
0.1	2	0.258	3.90×10^{-2}	0.233	0.234
0.03	4	1.87×10^{-5}	2.00×10^{-7}	1.993×10^{-5}	1.995×10^{-5}
0.0534	4	6.81×10^{-3}	2.63×10^{-4}	7.311×10^{-3}	7.313×10^{-3}
0.1	4	0.405	6.84×10^{-2}	0.4207	0.4209
0.03	6	2.94×10^{-5}	2.95×10^{-7}	2.756×10^{-5}	2.764×10^{-5}
0.0534	6	1.08×10^{-2}	3.91×10^{-4}	1.064×10^{-2}	1.065×10^{-2}
0.1	6	0.527	0.101	0.5830	0.5833

state vector from the solution of the TDSE we should try to minimize the right-hand side of Eq. (12).

C. Modified inhomogeneous evolution equation

Let us introduce the projection operator $\hat{P}$ with the kernel

$$\langle \boldsymbol{r}|\hat{P}|\boldsymbol{r}'\rangle = \sum_k \phi_k(\boldsymbol{r})\phi_k^*(\boldsymbol{r}'), \tag{18}$$

where $k \equiv n, l, m$ stands for the triples n, l, m of the quantum numbers of the bound states of the field-free atomic Hamiltonian with the coordinate representation wave functions $\phi_k(\boldsymbol{r})$. The operator $\hat{P}$ is a coordinate representation of the projection operator on the subspace of the Hilbert space spanned by the bound states of the field-free atomic Hamiltonian. We would like to have a modification of the SFA evolution equation (12) which would be more accurate and which, at the same time, would possess the appealing property of the SFA—the relative ease with which ionization amplitudes can be found. Such a modification (we shall call it SFAM below) can be achieved by modifying the right-hand side of Eq. (12) as follows:

$$i\frac{\partial \Psi_{\rm SFAM}(t)}{\partial t} - \hat{H}\Psi_{\rm SFAM}(t) = \hat{V}(\hat{P}\Psi_{\rm SFAM}(t) - \Psi_{\rm SFAM}(t)), \tag{19}$$

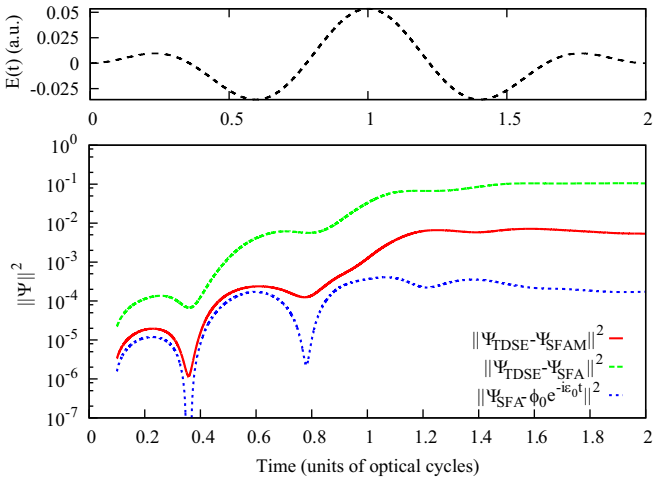

FIG. 1. Squared norms of the differences $||\Psi_{TDSE} - \Psi_{SFA}||^2$, $||\Psi_{TDSE} - \Psi_{\rm SFAM}||^2$, and $||\Psi_{SFA} - \phi_0 e^{-ie_0 t}||^2$ for the laser pulse with the peak field strength $E_0 = 0.0534$ a.u. and the total duration $T_1 = 2$ o.c. Inset shows the electric field of the pulse.

or in the equivalent form

$$i\frac{\partial \Psi_{\rm SFAM}(t)}{\partial t} - \hat{H}_F\Psi_{\rm SFAM}(t) = \hat{V}\hat{P}\Psi_{\rm SFAM}(t). \tag{20}$$

We may look at Eq. (20) as the TDSE with the true atomic potential $\hat{V}$ replaced with the effective potential $\hat{V}_{\rm eff} = \hat{V}\hat{P}$. Since this potential is non-Hermitian, the evolution described by Eq. (20) is nonunitary. We will see, nevertheless, that Eq. (20) can provide quite an accurate description of the ionization process. Appearance of the projection operator on the right-hand side of Eq. (19) is quite natural. As we mentioned above, to minimize the deviation of the approximate state vector from the solution of the TDSE the right-hand side of Eq. (12) should be made smaller. The right-hand side of Eq. (19) is indeed as small as possible provided we wish to retain the possibility of the relatively simple solution of an evolution equation even for complex systems. Indeed, evolution equation (19) can be solved with relatively little computational effort as follows.

Using the Volkov propagator (7) the solution to this equation with the initial condition $\Psi_{\rm SFAM}(0) = \phi_0$ can be written in integral form as

$$\Psi_{\rm SFAM}(t) = \hat{U}_F(t,0)\phi_0 - i\int_0^t \hat{U}_F(t,\tau)\hat{V}\hat{P}\Psi_{\rm SFAM}(\tau)\,d\tau, \tag{21}$$

where $\hat{H}_F = \hat{T} + \hat{H}_{\rm int}(t)$ is the Volkov Hamiltonian. We expand $\hat{P}\Psi_{\rm SFAM}(t)$ in Eq. (19) as

$$\hat{P}\Psi_{\rm SFAM}(t) = \sum_k a_k(t)\phi_k, \tag{22}$$

where ϕ_k are the bound-state wave functions of the atomic field-free Hamiltonian. Substituting this expansion in the right-hand side of Eq. (21), and projecting Eq. (21) on a bound atomic state ϕ_n, we obtain a system of the integral equations for the coefficients a_k in Eq. (22):

$$a_n(t) = \langle\phi_n|\hat{U}_F(t,0)|\phi_0\rangle - i\sum_k \int_0^t \langle\phi_n|\hat{U}_F(t,\tau)\hat{V}|\phi_k\rangle a_k(\tau)\,d\tau. \tag{23}$$

Calculation of the matrix elements in Eq. (23) does not present serious difficulties for any system for which the bound-state wave functions are known in the numerical form. Since computation of the matrix elements of the Volkov propagator is trivial in the plane-wave basis, the easiest way to

proceed is to use Fourier transforms of the bound-state wave functions. System (23) reduces then to a standard system of integral equations which can be easily solved providing the solution to Eq. (21), and hence to the evolution equation (19). It is clear from Eq. (21), Eq. (22), and Eq. (23) that this possibility to solve Eq. (19) relatively easily is the result of the presence of the projection operator $\hat{P}$ in the effective potential $\hat{V}_{\rm eff} = \hat{V}\hat{P}$.

As we mentioned above the evolution governed by Eq. (19) is nonunitary because of the presence of the non-Hermitian operator $\hat{V}_{\rm eff} = \hat{V}\hat{P}$ in the Hamiltonian. We may note that a different modification of Eq. (12) which makes the nonhomogeneous term on the right-hand side of Eq. (12) small, for which the modified evolution equation can still be solved with relative ease, and which would describe a unitary evolution, is possible. Instead of using the non-Hermitian effective potential $\hat{V}_{\rm eff} = \hat{V}\hat{P}$, we could use the effective potential $\hat{V}^{(1)}_{\rm eff} = \hat{P}\hat{V}\hat{P}$. Use of such a potential may have its advantages, unlike $\hat{V}_{\rm eff}$ the potential $\hat{V}^{(1)}_{\rm eff}$ is Hermitian; evolution driven by the corresponding evolution equation will, therefore, be unitary.

We will study below in detail the case of the non-Hermitian effective potential $\hat{V}_{\rm eff} = \hat{V}\hat{P}$ using hydrogen atom as an example. We solve the evolution equation (19) numerically, using the same modified matrix iteration method procedure we used to solve the SFA evolution equation (12). The projection operator (18) was defined using all the bound states with angular momentum $l_b \leqslant 12$ we obtain numerically by diagonalizing the discretized field-free atomic Hamiltonian.

To obtain the ionization probabilities once the evolution equation (19) has been solved on interval of the pulse duration we employ two different projection procedures. One follows the prescription encapsulated by Eq. (17), which relies on the projection of the wave function $\Psi_{\rm SFAM}(T_1)$ at the end of the pulse on the set of the ingoing scattering states of hydrogen. We will call the results obtained using this prescription the SFAM CP (SFAM with the Coulomb projection) results. We will also present below a set of the results obtained using a different projection procedure. One of the main goals of the present approach is to provide an algorithm allowing us to obtain relatively accurate values for the ionization probabilities with relative ease even for complex systems, e.g., the molecular systems. Exact scattering states for such systems may be difficult, if not impossible, to obtain. In such a situation we can use the projection on the plane-wave basis. Proper care, of course, must be taken of the nonorthogonality of the bound states of the system in question and the plane-wave states, which can be done as follows. Using the projection operator $\hat{P}$ introduced above, we first orthogonalize the solution of the SFAM evolution equation (19) taken at the end of the pulse to the subspace spanned by the bound states of the field-free Hamiltonian: $\tilde{\Psi}_{\rm SFAM}(T_1) = (\hat{I} - \hat{P})\Psi_{\rm SFAM}(T_1)$. We can use now the orthogonalized state vector $\tilde{\Psi}_{\rm SFAM}(T_1)$ to obtain the ionization amplitude:

$$a_{\boldsymbol{q}}^{PW} = \langle \boldsymbol{q}|\tilde{\Psi}_{\rm SFAM}(T_1)\rangle, \tag{24}$$

where $|\boldsymbol{q}\rangle$ is the plane-wave state with momentum $\boldsymbol{q}$, again normalized to $\delta(\boldsymbol{q} - \boldsymbol{q}')$. Results which this projection procedure gives are called below the SFAM PW results. We will also present below (mostly to illustrate effects due to the Coulomb interaction) some results obtained if the same procedure, consisting of orthogonalization of the solution of the evolution equation and projecting it on the plane-wave basis set, is applied to the solution of the SFA evolution equation (12). Projection on the plane-wave basis set is the method employed in the SFA, so using this projection prescription we come close to the orthodox SFA, with the only difference being that the SFA does not use the explicit orthogonalization procedure. For brevity, and permitting ourselves a slight abuse of the terminology, we will call below the results obtained using this projection prescription the SFA results.

III. RESULTS AND DISCUSSION

The accuracy which evolution equation (19) can provide is illustrated in Table I for the total ionization probabilities and in Figs. 2, 3, and 4 for the energy spectra. The SFAM calculation gives fairly accurate results for the total ionization probabilities, which agree well with the TDSE results. The improvement compared to the SFA results is dramatic, especially for the low field strengths in Table I, where the SFA and the TDSE results differ by two orders of magnitude. We note that SFAM CP and SFAM PW results agree very closely. This is, of course, an expected result for the total ionization probability. Indeed, by definition, the total ionization probability for the SFAM calculation can be expressed as $\langle\Psi_{\rm SFAM}(T_1)|\hat{Q}||\Psi_{\rm SFAM}(T_1)\rangle = ||\hat{Q}\Psi_{\rm SFAM}(T_1)||^2$, where $\hat{Q} = \hat{I} - \hat{P}$ is the projection operator on the continuous spectrum of the field-free Hamiltonian and $\Psi_{\rm SFAM}(T_1)$ is the SFAM vector of state at the end of the laser pulse. It is easy to see then that computing the total ionization probability as an integral $\int |a_{\boldsymbol{q}}|^2\, d\boldsymbol{q}$ in the case of the Coulomb projected amplitude (17), or $\int |\tilde{a}_{\boldsymbol{q}}|^2\, d\boldsymbol{q}$ for the plane-wave projected amplitude (24), we should get identical results because of the orthogonality of the bound and scattering states of the field-free Hamiltonian and by the unitary properties of the Coulomb and Fourier transforms, respectively. The differential ionization probabilities will generally differ, of course. In a numerical calculation, the total ionization probabilities can differ, since they are computed using different numerical procedures. Good agreement of the SFAM CP and SFAM PW data for the ionization probabilities in Table I is, therefore, a useful indication of the numerical accuracy we have achieved in our calculation. This is the reason why we present both sets of the data for the SFAM calculation in Table I. The same remark applies, of course, to total ionization probabilities obtained in the SFA CP and SFA calculations of the total ionization probabilities; they are equal within the small numerical inaccuracies. We do not present the SFA data in Table I, therefore. The better accuracy of the SFAM calculation comparing to the SFA CP results can also be observed in Fig. 2, where we had to scale the SFA CP results to facilitate the comparison with the TDSE and SFAM results.

A more detailed picture can be obtained by examining the finer characteristics, such as energy spectra and momentum distributions. The angle-integrated energy spectra in Figs. 2, 3, and 4 show that the agreement between SFAM and TDSE gets generally better for higher field strengths and longer pulses. As one see from the figures, for the field strengths of 0.0534 and 0.1 a.u. and the total pulse duration of 4 o.c. and 6 o.c.,

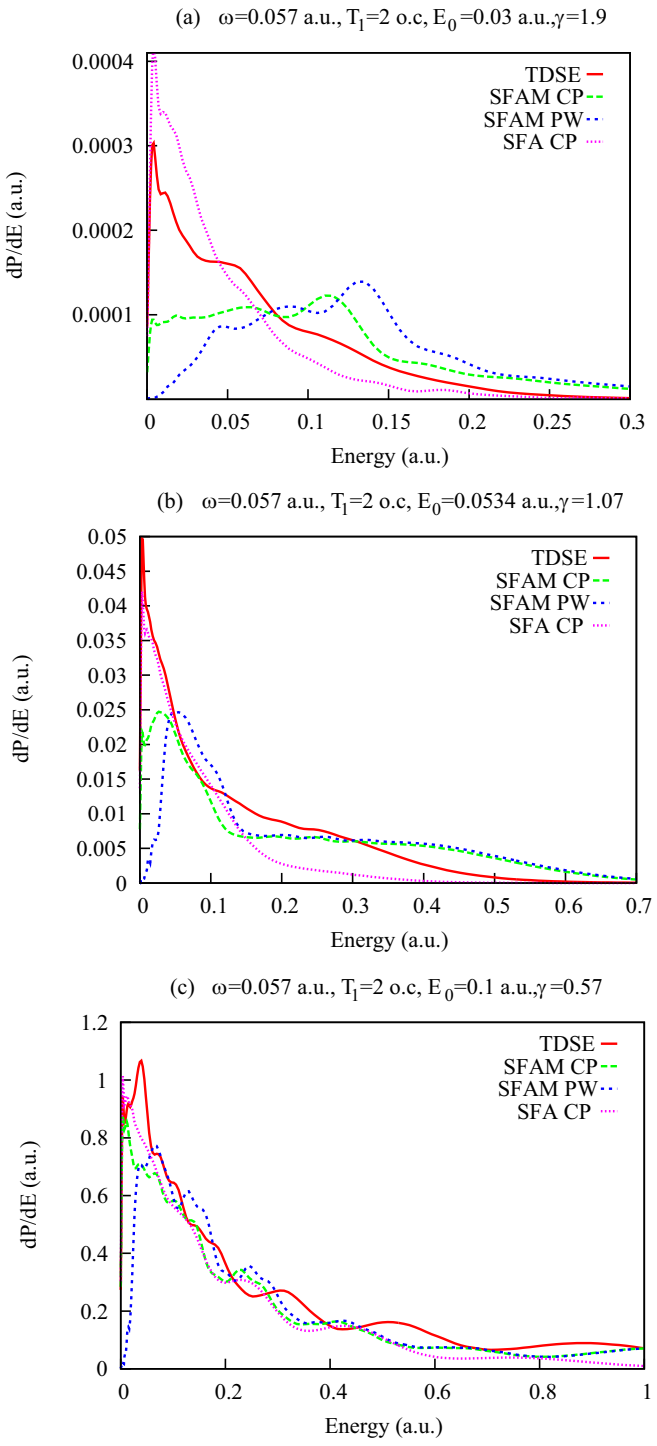

FIG. 2. Energy spectra obtained from the TDSE, SFAM, and SFA CP calculations for different field strengths and values of the Keldysh parameter γ. Pulse duration $T_1 = 2$ o.c. SFA CP results are scaled for better visibility by a factor of 100 (a), 20 (b), and 5 (c).

SFAM and TDSE energy spectra are in good agreement. One can see also that SFAM CP and SFAM PW spectra agree fairly well, except possibly the narrow region of very low energies $E \lesssim 0.1$ a.u. This could be anticipated since the low energies correspond to the parts of the ionized wave packet which at the moment $t = T_1$ of the end of the laser pulse stay near the ionic core, and it is the spatial region close to

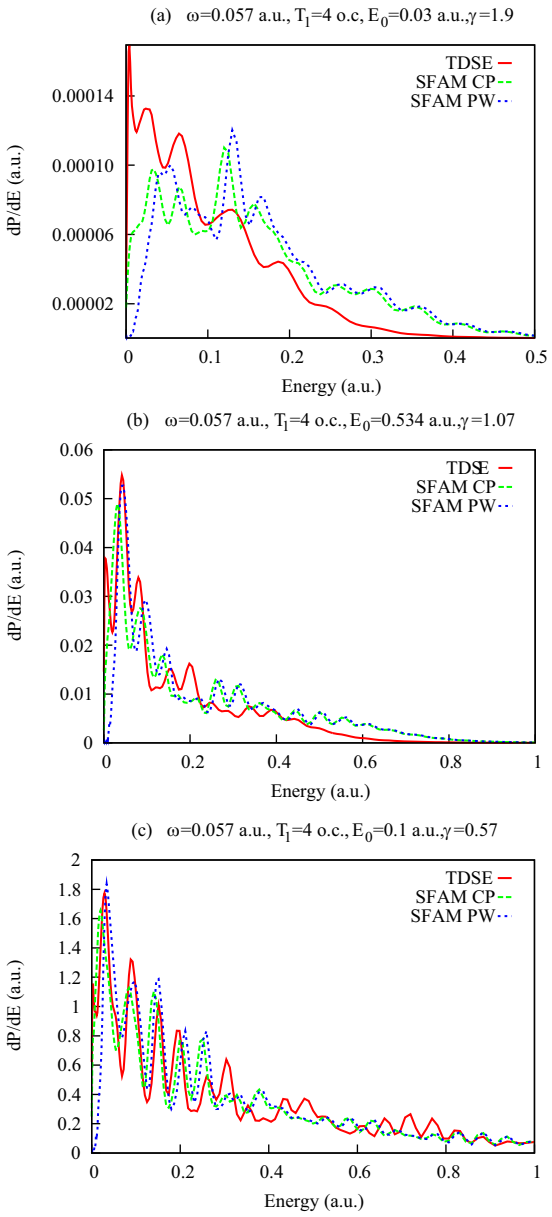

FIG. 3. Energy spectra obtained from the TDSE and SFAM calculations for different field strengths and values of the Keldysh parameter γ. Pulse duration $T_1 = 4$ o.c.

the core where the true scattering states and the plane-wave states differ substantially. One can see that the agreement between the SFAM CP and SFAM PW spectra at low energies gets better with the increasing pulse duration, when the small energy parts of the ionized wave packet have more time to travel away from the ionic core.

In Fig. 5 we show electron spectra for the different peak field strengths for a driving pulse of the 6 o.c. duration in a larger energy interval. These results support the conclusion we made above when we examined smaller energy interval: SFAM gets more accurate quantitatively with increasing field strength. As one can see from the figure, for the field strength of 0.1 a.u. the TDSE and SFAM spectra agree fairly well up to the energies of approximately $6U_p$, where the ponderomotive energy $U_p = E_0^2/4\omega^2 \approx 1$ a.u. for $E_0 = 1$ a.u. SFAM in this

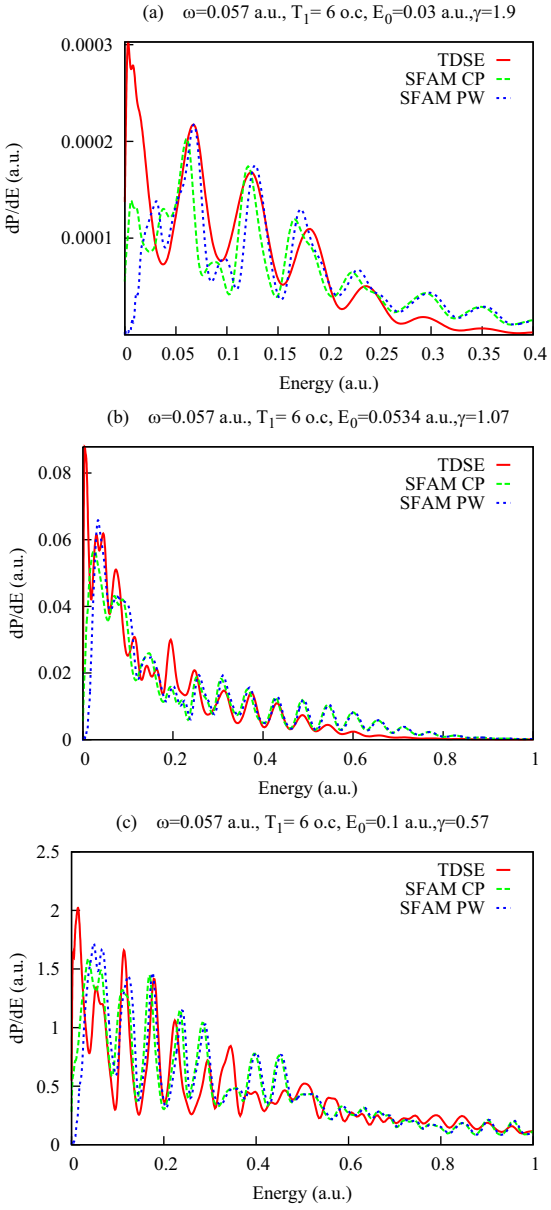

FIG. 4. Energy spectra obtained from the TDSE and SFAM calculations for different field strengths and values of the Keldysh parameter γ. Pulse duration $T_1 = 6$ o.c.

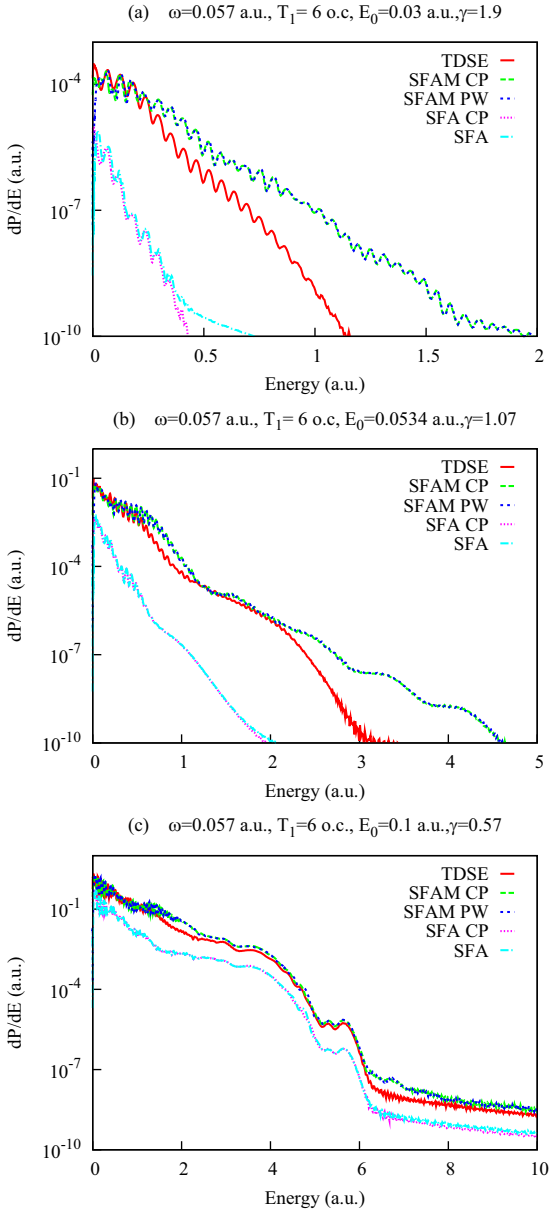

FIG. 5. Energy spectra obtained from the TDSE, SFAM, SFA CP, and SFA calculations for different field strengths and values of the Keldysh parameter γ in a larger energy interval. Pulse duration $T_1 = 6$ o.c.

case provides thus an adequate description of the directly ionized electrons (with the energies up to $2U_p$), and the rescattered electrons with larger energies. The effective potential $\hat{V}\hat{P}$ in Eq. (20) provides, therefore, a good description of the rescattering process responsible for the appearance of the electrons with energies exceeding $2U_p$ in the spectra. The SFAM CP and the SFAM PW results are virtually identical for the energy interval shown in Fig. 5, as well as the SFA CP and the SFA results, the two latter sets of the results differing considerably more from the results of the TDSE calculation than the SFAM data.

It is known that the ordinary SFA cannot describe a number of effects, which are the signatures of the Coulomb potential, such as the near-threshold structures in the angle-resolved spectra or the cusps in the transverse electron momentum distributions (TEMD) [15]. It is worthwhile to examine, therefore, to what extent the effective potential $\hat{V}\hat{P}$ in Eq. (20) can reproduce these structures. We show in Fig. 6 the transverse electron momentum distributions (TEMD) for the driving pulse with the total duration of 6 o.c. and different field strengths. For the geometry we employ, with the field polarized along the z direction, the TEMD can be obtained by integrating the triply differential ionization probability $P(p_x, p_y, p_z)$ over p_y and p_z. TEMD for the systems with long-range Coulomb interaction are known to exhibit cusps at the origin $p_\perp = p_x = 0$, which are signatures of the Coulomb focusing effect [15,26,27].

One can see from Fig. 6 that TEMD spectra given by the TDSE and SFAM CP calculations agree reasonably well

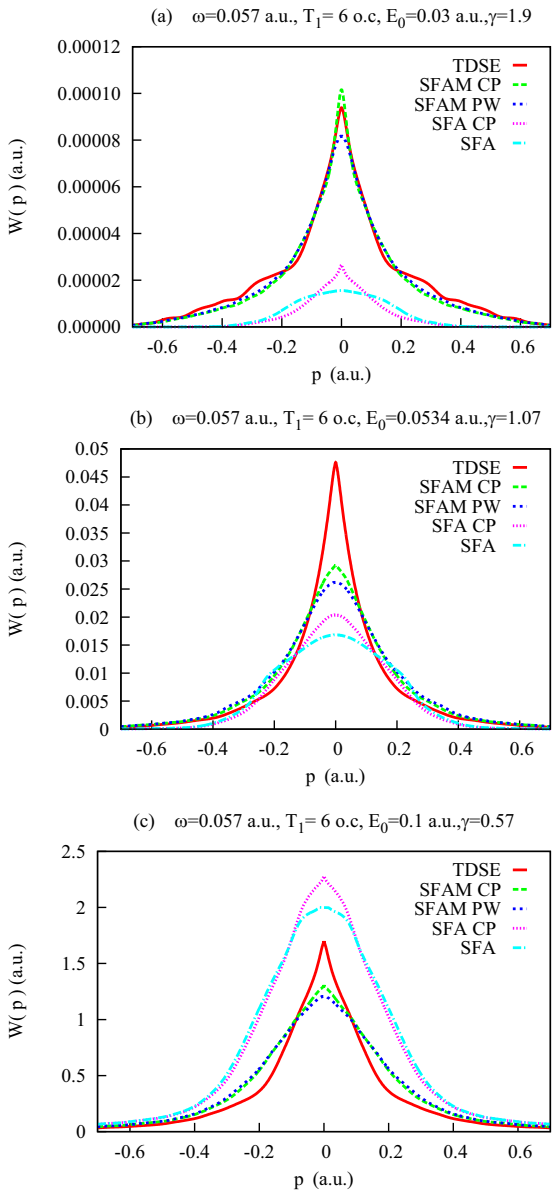

FIG. 6. Transverse electron momentum distributions obtained from the TDSE, SFAM, SFA CP, and SFA calculations for the different field strengths and the pulse duration $T_1 = 6$ o.c. SFA and SFA CP results are scaled for better visibility by a factor of 20 (a),(b) and 10 (c).

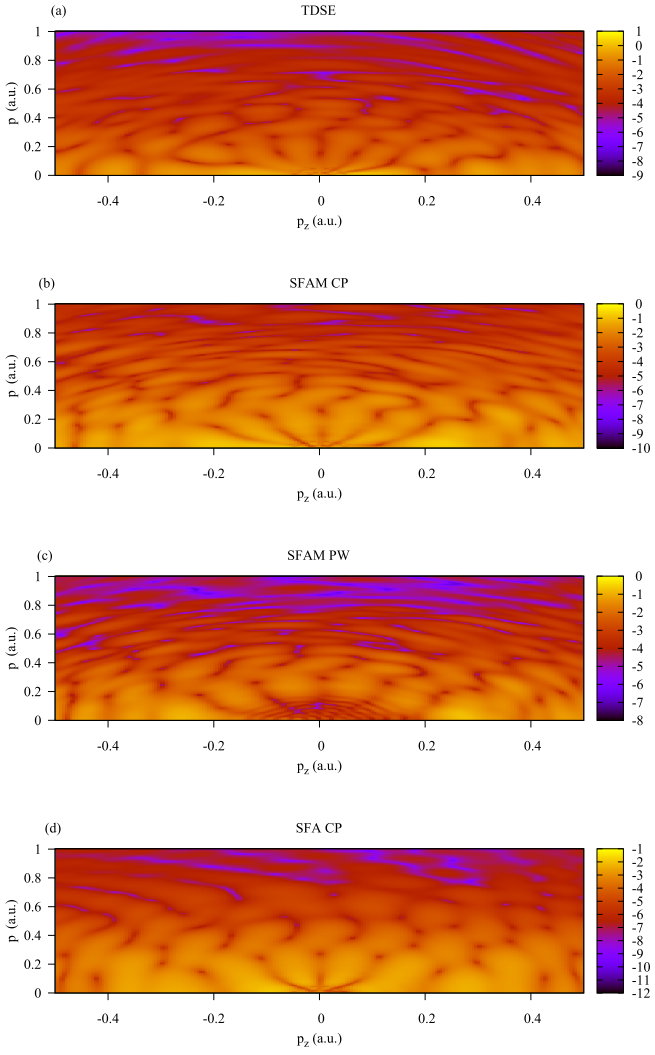

FIG. 7. Photoelectron momentum distribution in the cylindrical coordinates $(k_\perp, k_z)$ (logarithmic scale) for the TDSE, SFAM, and SFA CP calculations. Peak field strength $E_0 = 0.0534$ a.u.; pulse duration $T_1 = 6$ o.c.

both in shape and magnitude, the TEMD spectrum given by the SFAM CP calculation being slightly wider. This fact can be possibly explained by noting that the effective potential $\hat{V}_{\rm eff} = \hat{V}\hat{P}$ in Eq. (20) is weaker than the true atomic potential $\hat{V}$ in the following sense. The operator norm of the projection operator (18) is less than one, since for any projection operator with the range less than the total Hilbert space we must have $||\hat{P}|| < 1$. We have then $||\hat{V}_{\rm eff}|| < ||\hat{V}||$, meaning that effective potential is weaker, which results in a weaker focusing effect. We note that the SFAM PW calculation also reproduces the true TDSE TEMD fairly well, except the region near the small momenta, where it does not exhibit the cusp which is manifest in the TDSE and SFAM CP calculations. This is the consequence of the fact that, from the pure mathematical point of view, the origin of the cusp can be traced back to singularities of the Coulomb wave functions at zero energy [26,28], which are, of course, absent in the PW projection. The same effect can be observed by comparing the SFA CP and the SFA results which we also show in Fig. 6. The TEMD produced by the SFA shows the Gaussian structure which it inherits from the Gaussian structure of the 3D momenta distribution obtained in the SFA theory [20].

In Fig. 7 we show the comparison of the doubly differential electron momentum distributions $P(k_\perp, k_z)$ in the cylindrical coordinates $(k_\perp, k_z)$ for the pulse duration $T_1 = 6$ o.c. and peak field strength $E_0 = 0.0534$ a.u. The figure illustrates yet another feature of the momenta distributions—the near threshold structure (the so-called bouquet structure), which is known to be reproduced poorly by the SFA [15]. This structure results from the dominance of a single partial wave for the amplitude at small momenta which creates the characteristic pattern of the nodal lines near the origin of the $(k_\perp, k_z)$ plane. One can see that both the SFAM CP and SFAM PW calculations reproduce the bouquet structure of

the *ab initio* TDSE distribution much better than the SFA CP calculation. It is worth noting that, as we discussed above, the SFA CP results we present here are obtained by projecting the SFA time-dependent wave function (12) on the true scattering states of a hydrogen atom, not the plane-wave basis set as is usually done in the SFA calculations. In this respect, the SFA CP results we show here might be closer to the results of the so-called Coulomb-Volkov approximation (CVA) [15], which replaces the plane-wave basis set used for projection in the SFA with the set of the so-called Coulomb-Volkov functions, which take into account the effect of the Coulomb potential in the final state. It was shown [15] that the CVA generally reproduces the near threshold structures much better than the SFA. We see that, even with this improvement over the standard SFA, the SFA CP results we show in Fig. 7 are in not such good agreement with the TDSE results. SFAM results, on the contrary, are in a satisfactory agreement with the results of the *ab initio* TDSE calculation.

IV. CONCLUSIONS

We described a modification (SFAM) of the standard SFA method which partially takes into account the effects of the atomic potential. As Eq. (20) shows, this modification amounts to the use of the modified potential $\hat{V}\hat{P}$ instead of the true atomic potential $\hat{V}$, where $\hat{P}$ is the projection operator on the discrete spectrum of the field-free atomic Hamiltonian.

We recast both the standard SFA and the SFAM in the form of the time-dependent evolution equations. From this point of view, both these approximations are the nonhomogeneous evolution equations with the inhomogeneous term which determines the departure of the evolution driven by these equations from the evolution driven by the TDSE. The choice of the effective potential in Eqs. (19) and (20) was motivated, in fact, by the desire to make the right-hand side of the nonhomogeneous evolution equation, and hence the departure from the evolution driven by the true TDSE, smaller than in the case of the evolution equation for the SFA.

We compared the results of the SFA, SFAM, and TDSE calculations for different field parameters. We saw that SFAM gives pretty accurate (on the level of 20%–30%) values for the total ionization probabilities for a system with Coulomb interaction (a hydrogen atom). This is a dramatic improvement over the standard SFA, whose predictions for the total ionization probabilities can deviate from the TDSE by an order of magnitude or more. We saw that the effective potential $\hat{V}\hat{P}$ in the SFAM calculation also reproduces fairly accurately energy spectra, TEMD, and the near threshold structures in the double differential distributions. This is again an improvement over the SFA. It is important to note that these improvements have been achieved by keeping the main advantage of the SFA method—the relative simplicity with which results can be obtained. The evolution equation (20) can, as we saw, be solved relatively easily following the procedure encapsulated in Eq. (23). This procedure is equivalent to the direct solution of the nonhomogeneous evolution equation (20), and requires only the calculations of some matrix elements with the bound-state wave functions. Such calculations are quite feasible for any system for which the bound-state wave functions (or at least a sufficient number of them) can be obtained numerically. This fact, and the fact that SFAM's predictions, as we saw, compare pretty well with the *ab initio* TDSE for a hydrogen atom, can be used to obtain reliable quantitative information about the ionization of the systems for which the solution of the *ab initio* TDSE is not feasible, but the bound-states wave functions can be found relatively easily using known techniques, e.g., the molecular systems.

We used the length gauge in the calculations above. We could employ the velocity gauge in the SFA evolution equation (12), and obtain from it the velocity form of the SFAM evolution equation (20). Since both of these equations are only approximate evolution equations, the gauge invariance is broken. This means, in particular, that the evolution equations (20) using velocity and length forms are, in fact, two different approximations; corresponding time-dependent wave functions are not connected by a unitary transform as in the case of the exact *ab initio* TDSE. Which form of Eq. (20)—length or velocity—gives better results is an interesting question which can be answered only by detailed study. Further study may be required also to examine the unitary modification of the SFA which is obtained if we use the Hermitian effective potential $\hat{V}_{\rm eff}^{(1)} = \hat{P}\hat{V}\hat{P}$ to modify the SFA evolution equation. We reported a study of the results which the use of the non-Hermitian effective potential $\hat{V}_{\rm eff} = \hat{V}\hat{P}$ and the length form of the atom-field interaction gives, reserving the study of the velocity form and the unitary evolution driven by the Hermitian effective potential for future publications.

ACKNOWLEDGMENTS

This work was supported by IBS (Institute for Basic Science) under Grant No. IBS-R012-D1. I.A.I. benefited from useful discussions with S. V. Popruzhenko.

[1] L. V. Keldysh, Sov. Phys. JETP **20**, 1307 (1965).
[2] D. M. Wolkow, Z. Phys. **94**, 250 (1935).
[3] F. H. M. Faisal, J. Phys. B **6**, L89 (1973).
[4] H. R. Reiss, Phys. Rev. A **22**, 1786 (1980).
[5] A. M. Perelomov, V. S. Popov, and M. V. Terentiev, Sov. Phys. JETP **23**, 924 (1966).
[6] C. D. Lin, A.-T. Le, C. Jin, and H. Wei, J. Phys. B: At., Mol., Opt. Phys. **51**, 104001 (2018).
[7] P. B. Corkum, Phys. Rev. Lett. **71**, 1994 (1993).
[8] M. Lewenstein, K. C. Kulander, K. J. Schafer, and P. H. Bucksbaum, Phys. Rev. A **51**, 1495 (1995).
[9] O. I. Tolstikhin and T. Morishita, Phys. Rev. A **86**, 043417 (2012).
[10] M. Dörr and R. Shakeshaft, Phys. Rev. A **36**, 421(R) (1987).
[11] G. Duchateau, E. Cormier, and R. Gayet, Phys. Rev. A **66**, 023412 (2002).

[12] A. S. Kornev and B. A. Zon, J. Phys. B: At., Mol., Opt. Phys. **35**, 2451 (2002).
[13] J. Gagnon, F. Krausz, and V. S. Yakovlev, Phys. Rev. A **82**, 033435 (2010).
[14] O. Smirnova, V. S. Yakovlev, and M. Ivanov, Phys. Rev. Lett. **94**, 213001 (2005).
[15] D. G. Arbó, J. E. Miraglia, M. S. Gravielle, K. Schiessl, E. Persson, and J. Burgdörfer, Phys. Rev. A **77**, 013401 (2008).
[16] S. V. Popruzhenko, V. D. Mur, V. S. Popov, and D. Bauer, Phys. Rev. Lett. **101**, 193003 (2008).
[17] L. Torlina, M. Ivanov, Z. B. Walters, and O. Smirnova, Phys. Rev. A **86**, 043409 (2012).
[18] S. V. Popruzhenko, J. Phys. B: At., Mol., Opt. Phys. **47**, 204001 (2014).
[19] F. Krausz and M. Ivanov, Rev. Mod. Phys. **81**, 163 (2009).
[20] V. S. Popov, Phys. Usp. **47**, 855 (2004).
[21] I. A. Ivanov, Phys. Rev. A **90**, 013418 (2014).
[22] I. A. Ivanov and A. S. Kheifets, Phys. Rev. A **87**, 033407 (2013).
[23] M. Nurhuda and F. H. M. Faisal, Phys. Rev. A **60**, 3125 (1999).
[24] A. N. Grum-Grzhimailo, B. Abeln, K. Bartschat, D. Weflen, and T. Urness, Phys. Rev. A **81**, 043408 (2010).
[25] X. M. Tong, Z. X. Zhao, and C. D. Lin, J. Phys. B: At., Mol., Opt. Phys. **36**, 1121 (2003).
[26] A. Rudenko, K. Zrost, T. Ergler, A. B. Voitkiv, B. Najjari, V. L. B. de Jesus, B. Feuerstein, C. D. Schröter, R. Moshammer, and J. Ullrich, J. Phys. B: At., Mol., Opt. Phys. **38**, L191 (2005).
[27] A. N. Pfeiffer, C. Cirelli, A. S. Landsman, M. Smolarski, D. Dimitrovski, L. B. Madsen, and U. Keller, Phys. Rev. Lett. **109**, 083002 (2012).
[28] I. A. Ivanov, Phys. Rev. A **92**, 063417 (2015).